nature nanotechnology

LETTERS

PUBLISHED ONLINE: 4 JANUARY 2016 | DOI: 10.1038/NNANO.2015.291

Single-spin CCD

T. A. Baart[1†], M. Shafiei[1†], T. Fujita[1], C. Reichl[2], W. Wegscheider[2] and L. M. K. Vandersypen[1*]

Spin-based electronics or spintronics relies on the ability to store, transport and manipulate electron spin polarization with great precision[1–4]. In its ultimate limit, information is stored in the spin state of a single electron, at which point quantum information processing also becomes a possibility[5,6]. Here, we demonstrate the manipulation, transport and readout of individual electron spins in a linear array of three semiconductor quantum dots. First, we demonstrate single-shot readout of three spins with fidelities of 97% on average, using an approach analogous to the operation of a charge-coupled device (CCD)[7]. Next, we perform site-selective control of the three spins, thereby writing the content of each pixel of this 'single-spin charge-coupled device'. Finally, we show that shuttling an electron back and forth in the array hundreds of times, covering a cumulative distance of 80 μm, has negligible influence on its spin projection. Extrapolating these results to the case of much larger arrays points at a diverse range of potential applications, from quantum information to imaging and sensing.

Past experiments have shown macroscopic spin transport over distances exceeding 100 μm in clean bulk two-dimensional semiconductors[8,9]. Furthermore, controlled single-electron transport through semiconductor nanostructures[10] is now routine, with applications ranging from current standards to sensors and digital electronics[11]. Also, the controlled transfer of individual electrons between nanostructures separated by several micrometres has been realized[12,13]. However, the key combination of single-electron transport and spin preservation over large distances remains to be demonstrated.

A promising platform for moving around individual spins in a controlled manner is provided by analogy to a CCD[7]. In a CCD, pockets of electrical charge are passed along a capacitor array, which acts as a shift register, similar in spirit to a bucket-brigade. The pockets of charge arrive sequentially at the end of the array, where they are detected by a charge amplifier. This simple concept has enabled CCD cameras containing millions of pixels with applications from consumer electronics to astronomy[14]. The creation of an analogous device that can operate and detect single spins would also have powerful and diverse applications. For instance, it would not only enable reading out the outcome of a large quantum simulation or computation performed in a two-dimensional array of spins[6,15], but it could also be used for coherent imaging at the single photon level[16,17] or magnetic field sensing with 200 nm spatial resolution, using each single spin as a local probe. We term such a device a 'single-spin CCD'. Its operation requires the ability to shuttle spins one by one along a chain of sites without disturbing the spin states, and to record the state of the spin at the end of the chain.

We have created a prototype single-spin CCD using a linear triple-quantum-dot array. The array was formed electrostatically in a two-dimensional electron gas (2DEG) 85 nm below the surface (Fig. 1a). Gate electrodes fabricated on the surface of a GaAs/AlGaAs heterostructure (see Methods) were biased with appropriate voltages to selectively deplete regions of the 2DEG and define the linear array of three quantum dots. Each dot was initially occupied with one electron, with each of the three electrons constituting a single spin-1/2 particle. The sensing dot (SD) next to the quantum dot array was used for non-invasive charge sensing using radiofrequency (RF) reflectometry to monitor the number of electrons in each dot[18]. An in-plane magnetic field $B_{\text{ext}} = 3.51$ T was applied to split the spin-up (↑) and spin-down (↓) states of each electron by the Zeeman energy ($E_Z \approx 87$ μeV), defining a qubit in each of the dots. The electron temperature was 75 mK.

The CCD was initialized by loading ↑-spins from the right reservoir to every dot, as described in the schematic diagrams in Fig. 1b, which were implemented by the pulse sequence depicted by the arrows in Fig. 1c,d. Once the desired spin manipulation had been performed in the (1,1,1) regime, the readout sequence was started. This sequence followed the reverse path from the loading sequence, with the addition of three readout positions (denoted by green circles). As in a CCD, the three electrons were pushed sequentially to the readout site at the end of the chain. First, the right dot was tuned to the position of green circle '3' in Fig. 1d. At this position, an excited spin-↓ electron was allowed to tunnel to the reservoir, while a ground-state spin-↑ electron would remain in the dot. The nearby sensing dot was used to record whether or not the electron had tunnelled out, revealing its spin state[19]. Next, the gate voltages were adjusted to shuttle the centre electron to the right dot for readout, at the position of green circle '2'. Subsequently, the left spin was shuttled through the centre dot to the right, completing the three-spin readout at the position of green circle '1' in Fig. 1c. For details see Supplementary Section II 'Detailed information of the applied pulse sequence'.

The operation of the single-spin CCD was tested by preparing various combinations of the eight three-spin populations ↑↑↑ to ↓↓↓. To achieve this, we carried out site-selective manipulation of each of the three spins by exploiting the small difference in g factors between the dots (Fig. 2i) combined with adiabatic inversion of the spins using electric dipole spin resonance (EDSR)[20]. This amounts to 'writing' the qubits of the single-spin CCD. After loading ↑↑↑, we thus created spin states ↓↑↑, ↑↓↑ or ↑↑↓, and subsequently varied the waiting time in the (1,1,1) configuration. During that time, the populations evolved as the spins relaxed back to the ground state ↑↑↑.

Figure 2a–h shows the eight three-spin probabilities as a function of waiting time for the three initial state preparations. Data are also shown where random spins are injected into each of the three dots. We see that the data closely follow the expected behaviour (see Fig. 2 caption), shown as solid lines, indicating proper operation of the single-spin CCD.

This is the first demonstration of reading out multiple spins through the same reservoir. Readout fidelities are on average 98.2 (±0.5)% for spin-up and 95.8 (±0.3)% for spin-down (Supplementary Section I 'Calculation of the fidelities').

We next examine the effect of shuttling electrons between dots on their spin projection. We anticipate that three mechanisms

[1]QuTech and Kavli Institute of Nanoscience, TU Delft, GA Delft 2600, The Netherlands. [2]Solid State Physics Laboratory, ETH Zürich, Zürich 8093, Switzerland. [†]These authors contributed equally to this work. *e-mail: l.m.k.vandersypen@tudelft.nl

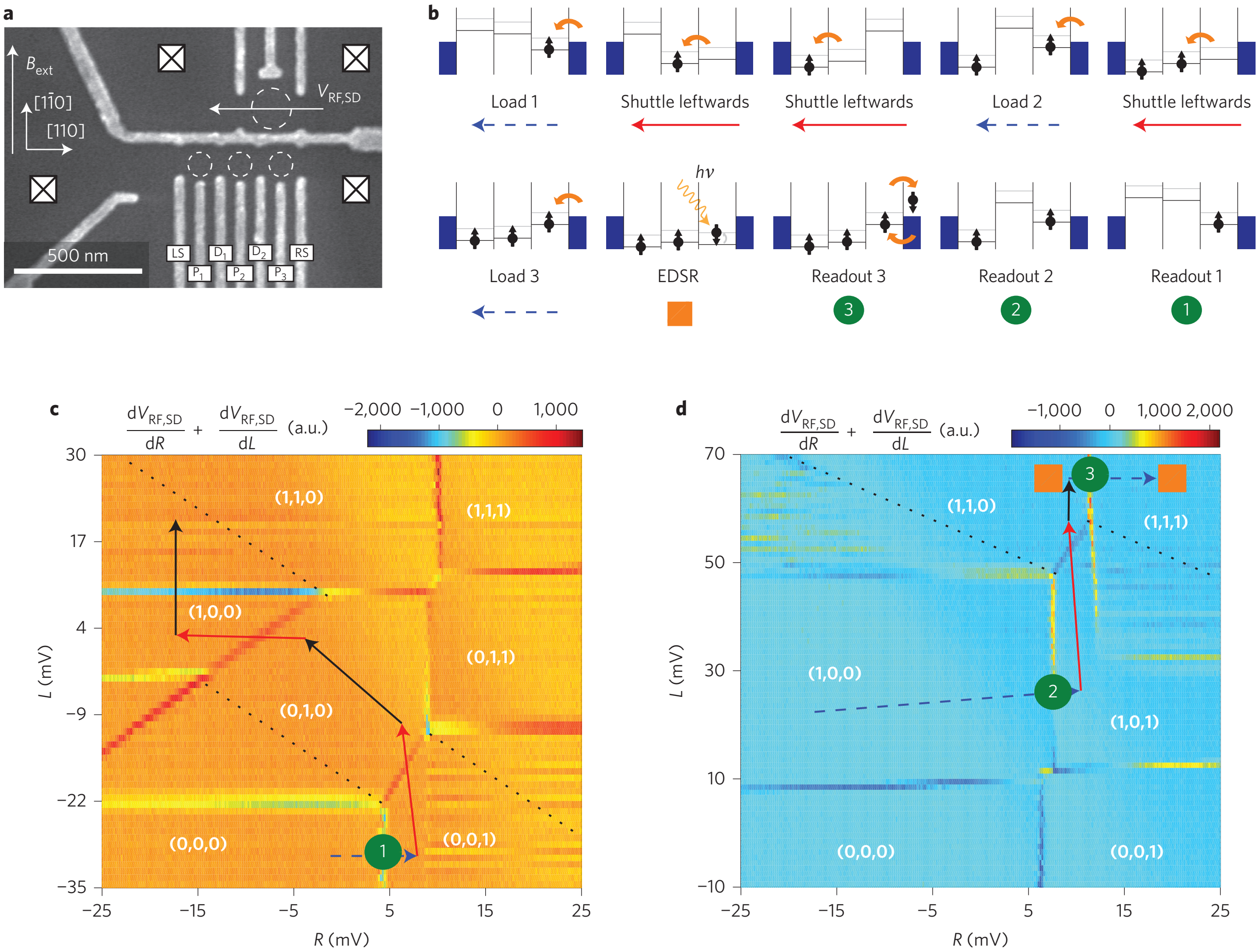

Figure 1 | Linear array of three quantum dots and single-spin CCD operation. a, Scanning electron microscopy image of a sample nominally identical to the one used for the measurements. Dashed circles indicate quantum dots and squares indicate Fermi reservoirs in the 2DEG, which are connected to ohmic contacts. The RF reflectance of the SD is monitored to determine the occupancies of the triple dot. **b**, Read from left to right and top to bottom. The CCD is initialized by loading three electrons from the right reservoir and shuttling them to their final position (analogous to a shift register). We load ↑-spins by ramping slowly through the charge transition lines with the right reservoir (slow compared with the tunnel rate with the reservoir). Single-spin manipulation can be performed through EDSR. Readout occurs using spin-selective tunnelling. **c**,**d**, Charge stability diagram of the triple dot for two different values of M (**c**, −42 mV; **d**, −56 mV). L, M and R are linear combinations of the voltages applied to gates P_1, P_2 and P_3, allowing us to partially compensate for cross-capacitances (Supplementary Section V 'Virtual gates L, M, R, and the usage of "fast honeycombs"'). L, M and R therefore couple mostly to the left, middle and right dots, respectively. The occupancy of each dot is denoted by (n,m,p), corresponding to the number of electrons in the left, middle and right dots, respectively. The fading of the middle dot charge transition lines can be explained in a similar way as in ref. 35 (black dotted lines indicate their positions). The pulse sequence for loading and readout is indicated in the charge stability diagrams by arrows (see also **b**). From **c** and **d** we pulse M, keeping L and R the same.

could, in principle, cause the spin projection to change: (1) charge exchange with the reservoirs, (2) a spin–orbit (SO) interaction and (3) hyperfine interaction with the nuclear spins of the quantum-dot host material. Mechanism (1) is suppressed by applying precisely tuned pulse sequences and keeping the tunnel barriers of the reservoirs sufficiently closed. For the present gate voltage settings, we estimate this error to be $<1\times10^{-5}$ per hop along the array (Supplementary Section IIIA 'Estimation of the error rate during shuttling'). The SO interaction (2) could affect the spin state, in a deterministic way, as it propagates through the array[21,22]. The direction of movement with respect to the crystal axis determines the magnitude and direction of the SO field. We expect the SO interaction to be largest for motion along the [1$\bar{1}$0] axis and minimal along the interdot axis [110][23,24] (Fig. 1a). Furthermore, the small SO field still originating from movement along this interdot axis will be parallel to the external field and therefore will not influence the spin projection. The hyperfine interaction (3) can cause random flips arising from the instantaneous unknown difference in perpendicular (relative to B_{ext}) hyperfine field, $\delta B_\perp$, between neighbouring dots. This effect is suppressed by the large B_{ext} and is estimated to be $<1\times10^{-6}$ per shuttle event assuming $\delta B_\perp < 7$ mT (Supplementary Section IIIB 'Estimation of the error rate during shuttling'). In future experiments, mechanisms (2) and (3) could be further suppressed by transferring the spin from one dot to the other adiabatically when compared to the Zeeman splitting.

To verify experimentally whether it is possible to shuttle electrons while preserving their spin projection, we simulated a very large array using the triple dot device. Using the charge states from Fig. 1c, we loaded one random electron in the (0,0,1) state and shuttled it back and forth many times to (1,0,0) by passing through (0,1,0) as depicted schematically in Fig. 3b. Each run of going back and forth constitutes a total of four jumps from one dot to the other. In Fig. 3a, both the total time spent in the CCD, t_{CCD}, and the number of interdot hops, n_{hops}, are varied and the spin read out at the end. Up to 20, 70 and 350 hops, for t_{CCD} values of 2, 7 and 35 ms, respectively, the time between jumps is longer than the timescale on which the

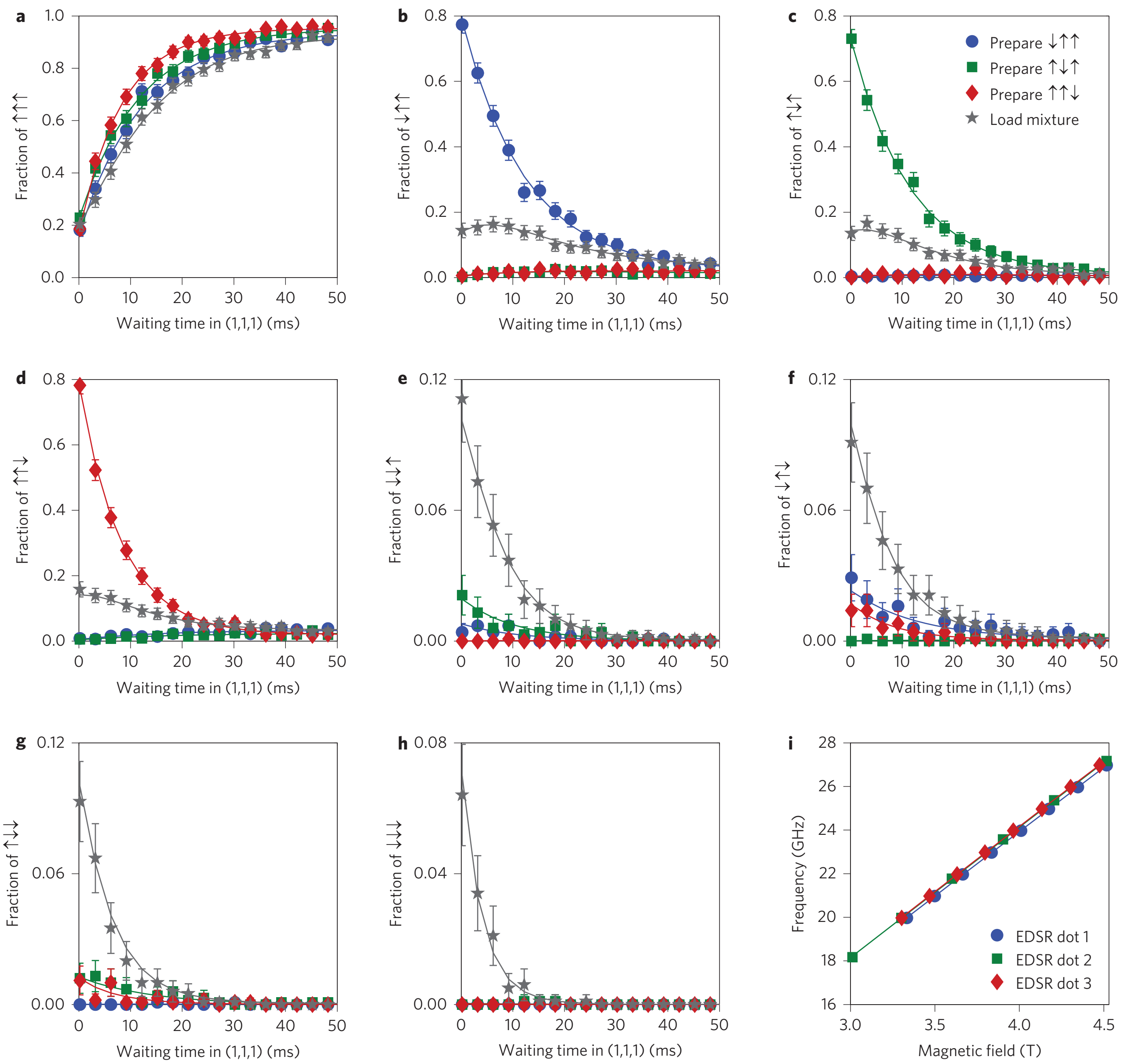

Figure 2 | Writing and readout of the single-spin CCD. a–h, Measured three-spin populations as a function of waiting time between state preparation and readout for four different state preparations. Starting from ↑↑↑ (>95% initialization efficiency), states ↓↑↑ (blue) and ↑↑↓ (red) are prepared by EDSR in the (1,1,1) regime. State ↑↓↑ (green) is created by applying EDSR in the (1,1,0) regime, and then loading the third ↑-spin. For fourth state preparation, the gate voltages are not ramped but pulsed across the relevant charge transitions, so that electrons with random spin will occupy the three dots. The contrast is limited to 0.8 mostly by imperfect adiabatic inversion and not by the readout fidelities. Each data point is an average of 999 measurements (error bars indicate two standard deviations, s.d.). Solid lines are products of the calculated single-spin probabilities based on the individual T_1 and initial spin-down probability of each dot. The fact that they overlap with the corresponding three-spin probabilities demonstrates that no (unintended) correlations were introduced between the spins. **i**, Resonance frequency for each dot i as a function of the magnetic field. A fit of the form $f_{res} = (g_1^i \mu_B B/h) + (g_3^i \mu_B B^3/h)$[36], where μ_B is the Bohr magneton and h is Planck's constant, gives $g_1^1 = -0.430 \pm 0.001$, $g_1^2 = -0.434 \pm 0.003$ and $g_1^3 = -0.434 \pm 0.002$. Despite similar g_1 factors in dots 2 and 3, time variations of the local nuclear field still give rise to stable configurations where we can selectively address the two dots (see also Supplementary Section VI 'EDSR spectra of each dot and spin-down initialization efficiencies' for g_3^i).

transverse component of the local nuclear field is randomized, which is the nuclear spin coherence time (~100 μs for the nuclear spins[25]). This prevents coherent error accumulation as an electron repeatedly hops between the same dots. In that case, the effect of moving back and forth in the triple dot is the same as traversing successive dots in the same direction. For a larger number of hops and a fixed t_{CCD}, the hopping rate increases and correlations may build up, although we have no indication of such an effect occurring in the present experiments. Fitting the data for each t_{CCD} to a linear curve gives an average change in the spin-down fraction ranging between -1.7×10^{-6} and $+8.3 \times 10^{-6}$ per hop (Supplementary Section IIIA 'Estimation of the error rate during shuttling'). We compared the measured spin state after shuttling many times, with the spin state measured after the electron had shuttled back and forth only once in exactly the same total amount of time. The latter effectively constitutes a weighted T_1 measurement over the three dots. The fact that the triangular symbols in Fig. 3a fall exactly on the weighted T_1 decay indicates that there is no sign of spin flips other than through spontaneous relaxation, even after more than 500 hops. Taking an interdot distance of 160 nm, this corresponds to a total distance of ~80 μm.

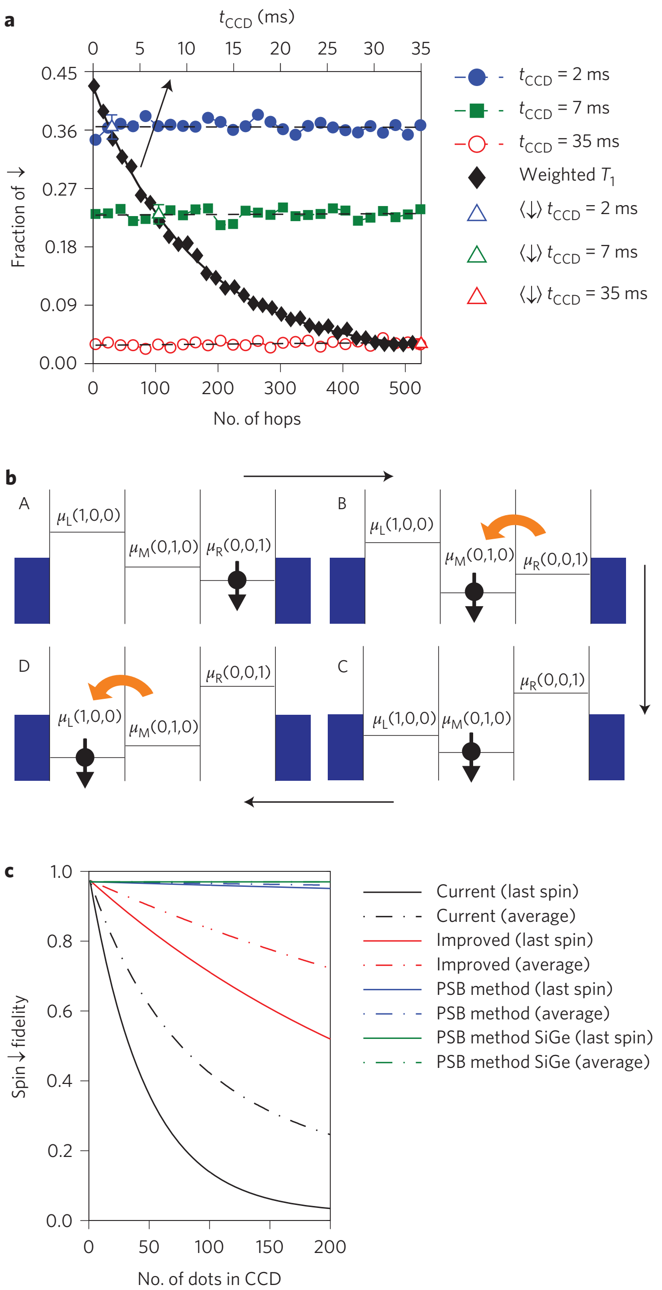

Figure 3 | Preservation of the spin projection during shuttling. a, Circles and squares: measured spin-down probability after n_{hops} interdot hopping events for three values of total time t_{CCD}. Black dashed lines are linear fits to the data. Diamonds: measured spin-down probability after shuttling back and forth just once, as a function of total shuttling time t_{CCD}. The decay time constant represents a weighted T_1 over all three dots ($T_{1,\mathrm{weighted}}$ = 10.6 ± 0.5 ms). Triangles depict the average value of the shuttling data (circles and squares) for each value of t_{CCD} (error bars indicate 2 s.d.). **b**, Schematic representation of the tunnelling of a spin back and forth inside the CCD array. Arrows depict the backwards trajectory from the right to the left dot. Reversing this pathway returns the spin to the right dot. There are two separate stages with the electron in the middle dot, to prevent charge exchange with the reservoirs (Supplementary Section IIIA 'Estimation of the error rate during shuttling'). **c**, Estimated spin-down measurement fidelity as a function of the length of the single-spin CCD for the current settings, improved conditions as described in the main text, and for the proposed PSB scheme in GaAs and SiGe. Solid lines indicate the fidelity for the spin that is read out last, and dashed lines indicate the average fidelity for the whole array. The spin-up fidelity is independent of CCD size.

An important question to address is the scalability of this approach. A single SD is not capable of recording charge stability diagrams, such as in Fig. 1c, for arrays much larger than three dots. However, by implementing dispersive gate sensors[26], one can first detect the required charge transitions to implement the shuttle scheme without requiring additional SDs. This approach is also well suited to two-dimensional arrays. The data in Fig. 3a show that in the current experiment, the bottleneck for improving the readout fidelities is not the shuttling of the spins itself, but rather relaxation while waiting for readout. More specifically, the limiting factors for this experiment are the time it takes to read out (~130 μs) and to empty a dot (~75 μs), and the time allowed for shuttling to the next dot (~10 μs). The black curves in Fig. 3c show the predicted spin-down fidelity as a function of the CCD length, extrapolated based on the present numbers.

With a few technical improvements involving additional pulse lines, larger interdot tunnel couplings and a somewhat lower magnetic field, tunnelling and emptying can occur on a nanosecond timescale, the readout time can be halved, and T_1 can be doubled (Supplementary Section IV 'Suggested improvements to increase the read-out fidelities'). This would give fidelities as shown in red in Fig. 3c, allowing one to read out 50 spins with >83% fidelity.

The readout time can be shortened more dramatically by the inclusion of Pauli spin blockade (PSB) in the readout scheme. PSB allows one to distinguish whether two neighbouring spins are parallel or anti-parallel[27,28]. PSB readout within 1 μs for a fidelity of 97% has been demonstrated in GaAs dots[29]. To implement this method in future experiments for readout of a number of spins in as many dots, we suggest adding, from the right, an empty dot and a dot occupied by one electron, which will act as an ancillary reference spin. In this way, one can quickly initialize the reference spin in the ↑-state on the rightmost dot using a so-called hotspot where spins relax on a sub-microsecond timescale[30,31]. The first spin to be read out will then be shuttled to the empty dot next to the reference spin and its spin is determined using PSB. After discarding one of the spins, the remaining spin will be reinitialized to be spin-up again, and the procedure will be repeated until the whole chain of spins has been read out. This procedure significantly reduces the readout time, leading to the blue curve in Fig. 3c, with fidelities above 88% for arrays of 1,000 spins. Moving to a different host material such as Si or SiGe, T_1 times can reach seconds[31,32], boosting fidelities further (green curve). For such large T_1 times, we estimate that the readout fidelity of the last spin that is read out in an array of 1,000 dots will decrease by only 0.07% compared to the readout fidelity of the first spin.

The high fidelity with which the spin projection can be preserved upon shuttling between dots thus allows scaling the single-spin CCD concept to linear arrays of hundreds of dots. Two-dimensional arrays would be a natural next step. This would require either the use of weak spin–orbit materials like silicon, or accounting for (predictable) spin–orbit-induced rotations along at least one direction. Finally, in materials with negligible hyperfine coupling, such as ^{28}Si-enriched substrates[33], not only the spin projection but also the spin phase is expected to be preserved during shuttling. Such coherent single-spin shuttles allow qubits to be moved in the course of a quantum computation, an essential tool for powerful quantum computing architectures[6,34].

Methods

Methods and any associated references are available in the online version of the paper.

Received 13 July 2015; accepted 11 November 2015; published online 4 January 2016

References

1. Prinz, G. A. Spin-polarized transport. *Phys. Today* **48,** 58–63 (1995).
2. Wolf, S. A. *et al.* Spintronics: a spin-based electronics vision for the future. *Science* **294,** 1488–1495 (2001).

3. Žutić, I., Fabian, J. & Sarma, S. D. Spintronics: fundamentals and applications. *Rev. Mod. Phys.* **76,** 323–410 (2004).
4. Spintronics insight. *Nature Mater.* **11,** 367–416 (2012).
5. Hanson, R. & Awschalom, D. D. Coherent manipulation of single spins in semiconductors. *Nature* **453,** 1043–1049 (2008).
6. Taylor, J. M. *et al.* Fault-tolerant architecture for quantum computation using electrically controlled semiconductor spins. *Nature Phys.* **1,** 177–183 (2005).
7. Boyle, W. S. & Smith, G. E. Charge coupled semiconductor devices. *Bell Syst. Tech. J.* **49,** 587–593 (1970).
8. Kikkawa, J. & Awschalom, D. Lateral drag of spin coherence in gallium arsenide. *Nature* **397,** 139–141 (1999).
9. Crooker, S. A. *et al.* Imaging spin transport in lateral ferromagnet/semiconductor structures. *Science* **309,** 2191–2195 (2005).
10. Grabert, H. & Devoret, M. H. (eds) *Single Charge Tunneling* Vol. 294 (NATO ASI Series, Springer, 1992).
11. Ono, Y., Fujiwara, A., Nishiguchi, K., Inokawa, H. & Takahashi, Y. Manipulation and detection of single electrons for future information processing. *J. Appl. Phys.* **97,** 031101 (2005).
12. McNeil, R. P. G. *et al.* On-demand single-electron transfer between distant quantum dots. *Nature* **477,** 439–442 (2011).
13. Hermelin, S. *et al.* Electrons surfing on a sound wave as a platform for quantum optics with flying electrons. *Nature* **477,** 435–438 (2011).
14. Howell, S. B. *Handbook of CCD Astronomy* (Cambridge Univ. Press, 2006).
15. Barthelemy, P. & Vandersypen, L. M. K. Quantum dot systems: a versatile platform for quantum simulations. *Ann. Phys. (Leipz.)* **525,** 808–826 (2013).
16. Vrijen, R. & Yablonovitch, E. A spin-coherent semiconductor photo-detector for quantum communication. *Physica E* **10,** 569–575 (2001).
17. Fujita, T. *et al.* Nondestructive real-time measurement of charge and spin dynamics of photoelectrons in a double quantum dot. *Phys. Rev. Lett.* **110,** 266803 (2013).
18. Barthel, C. *et al.* Fast sensing of double-dot charge arrangement and spin state with a radio-frequency sensor quantum dot. *Phys. Rev. B* **81,** 3–6 (2010).
19. Elzerman, J. M. *et al.* Single-shot read-out of an individual electron spin in a quantum dot. *Nature* **430,** 431–435 (2004).
20. Shafiei, M., Nowack, K., Reichl, C., Wegscheider, W. & Vandersypen, L. Resolving spin–orbit- and hyperfine-mediated electric dipole spin resonance in a quantum dot. *Phys. Rev. Lett.* **110,** 107601 (2013).
21. Danon, J. & Nazarov, Y. V. Pauli spin blockade in the presence of strong spin–orbit coupling. *Phys. Rev. B* **80,** 041301 (2009).
22. Schreiber, L. *et al.* Coupling artificial molecular spin states by photon-assisted tunnelling. *Nature Commun.* **2,** 556 (2011).
23. Golovach, V. N., Khaetskii, A. & Loss, D. Phonon-induced decay of the electron spin in quantum dots. *Phys. Rev. Lett.* **93,** 016601 (2004).
24. Scarlino, P. *et al.* Spin-relaxation anisotropy in a GaAs quantum dot. *Phys. Rev. Lett.* **113,** 256802 (2014).
25. Hanson, R. *et al.* Spins in few-electron quantum dots. *Rev. Mod. Phys.* **79,** 1217–1265 (2007).
26. Colless, J. I. *et al.* Dispersive readout of a few-electron double quantum dot with fast RF gate sensors. *Phys. Rev. Lett.* **110,** 046805 (2013).
27. Ono, K., Austing, D. G., Tokura, Y. & Tarucha, S. Current rectification by Pauli exclusion in a weakly coupled double quantum dot system. *Science* **297,** 1313–1317 (2002).
28. Nowack, K. C., Koppens, F. H., Nazarov, Y. V. & Vandersypen, L. M. K. Coherent control of a single electron spin with electric fields. *Science* **318,** 1430–1433 (2007).
29. Shulman, M. D. *et al.* Demonstration of entanglement of electrostatically coupled singlet–triplet qubits. *Science* **336,** 202–205 (2012).
30. Srinivasa, V., Nowack, K. C., Shafiei, M., Vandersypen, L. M. K. & Taylor, J. M. Simultaneous spin-charge relaxation in double quantum dots. *Phys. Rev. Lett.* **110,** 196803 (2013).
31. Yang, C. H. *et al.* Spin–valley lifetimes in a silicon quantum dot with tunable valley splitting. *Nature Commun.* **4,** 2069 (2013).
32. Simmons, C. B. *et al.* Tunable spin loading and T1 of a silicon spin qubit measured by single-shot readout. *Phys. Rev. Lett.* **106,** 156804 (2011).
33. Veldhorst, M. *et al.* An addressable quantum dot qubit with fault-tolerant control fidelity. *Nature Nanotech.* **9,** 981–985 (2014).
34. Kielpinski, D., Monroe, C. & Wineland, D. J. Architecture for a large-scale ion-trap quantum computer. *Nature* **417,** 709–711 (2002).
35. Yang, C. H. *et al.* Charge state hysteresis in semiconductor quantum dots. *Appl. Phys. Lett.* **105,** 183505 (2014).
36. Shafiei, M. *Electrical Control, Read-out and Initialization of Single Electron Spins* PhD thesis, Delft Univ. of Technology (2013).

Acknowledgements
The authors acknowledge useful discussions with the members of the Delft spin qubit team, sample fabrication by F.R. Braakman and experimental assistance from M. Ammerlaan, A. van der Enden, J. Haanstra, R. Roeleveld, R. Schouten, M. Tiggelman and R. Vermeulen. This work is supported by the Netherlands Organization of Scientific Research (NWO) Graduate Program, the Intelligence Advanced Research Projects Activity (IARPA) Multi-Qubit Coherent Operations (MQCO) Program and the Swiss National Science Foundation.

Author contributions
T.A.B., M.S. and T.F. performed the experiment and analysed the data. C.R. and W.W. grew the heterostructure. T.A.B., M.S., T.F. and L.M.K.V. contributed to interpretation of the data and commented on the manuscript. T.A.B. and L.M.K.V. wrote the manuscript.

Additional information
Supplementary information is available in the online version of the paper. Reprints and permissions information is available online at www.nature.com/reprints. Correspondence and requests for materials should be addressed to L.M.K.V.

Competing financial interests
The authors declare no competing financial interests.

Methods

The experiment was performed on a $GaAs/Al_{0.25}Ga_{0.75}As$ heterostructure grown by molecular-beam epitaxy, with an 85-nm-deep 2DEG with an electron density of 2.0×10^{11} cm^{-2} and mobility of 5.6×10^{6} cm^{2} V^{-1} s^{-1} at 4 K. The metallic (Ti–Au) surface gates were fabricated using electron-beam lithography. The main function of gates LS and RS was to set the tunnel coupling with the left and right reservoirs, respectively. D_1 and D_2 controlled the interdot tunnel coupling and P_1, P_2 and P_3 were used to set the electron number in each dot. The device was cooled inside an Oxford Kelvinox 400HA dilution refrigerator to a base temperature of 45 mK. To reduce charge noise, the sample was cooled while applying a positive voltage on all gates (ranging between 0 and 350 mV)[37]. The device was tuned in the single-electron regime. The tunnel coupling at zero detuning between dots 1 and 2 was measured to be 0.8 and 0.5 GHz between dots 2 and 3 using photon-assisted tunnelling[38]. Gates P_1, P_2, P_3 and D_2 were connected to homebuilt bias-tees (RC = 470 ms), enabling application of a d.c. voltage bias as well as high-frequency voltage excitation to these gates. RF reflectometry of the SD was performed using an LC circuit matching a carrier wave of frequency 110.35 MHz. The inductor was formed from a microfabricated NbTiN superconducting spiral inductor with an inductance of 3.0 μH. The power of the carrier wave arriving at the sample was estimated to be −99 dBm. The carrier signal was only unblanked during readout. The reflected signal was amplified using a cryogenic Weinreb CITLF2 amplifier and subsequently demodulated using homebuilt electronics. Real-time data acquisition was performed using a field-programmable gate array (FPGA) (DE0-Nano Terasic) programmed to detect tunnel events using a Schmidt trigger. The microwaves were generated using an HP83650A connected to P_2 via a homemade bias-tee at room temperature. Voltage pulses to the gates were applied using a Tektronix AWG5014 (0–100% rise time = 5 ns).

References

37. Long, A. R. *et al*. The origin of switching noise in GaAs/AlGaAs lateral gated devices. *Physica E* **34,** 553–556 (2006).
38. Oosterkamp, T. H. *et al*. Microwave spectroscopy of a quantum-dot molecule. *Nature* **395,** 873–876 (1998).